

pubs.acs.org/cm Article

Controlled Assembly of Icosahedral Colloidal Clusters for Structural Coloration

Cheolho Kim, $^{\nabla}$ Kinam Jung, $^{\nabla}$ Ji Woong Yu, $^{\nabla}$ Sanghyuk Park, Shin-Hyun Kim, Won Bo Lee, Hyerim Hwang,* Vinothan N. Manoharan,* and Jun Hyuk Moon*



Cite This: Chem. Mater. 2020, 32, 9704-9712



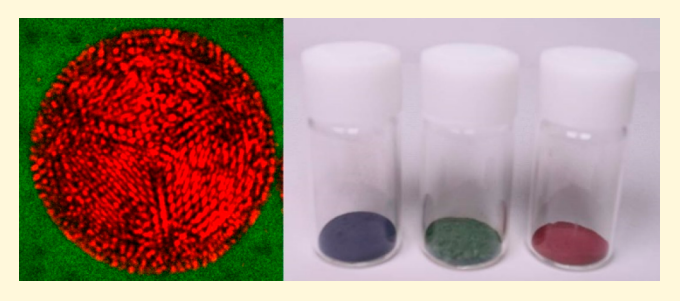
ACCESS

Metrics & More



Supporting Information

ABSTRACT: Icosahedral colloidal clusters are a new class of spherical colloidal crystals. This cluster allows for potentially superior optical properties in comparison to conventional onion-like colloidal supraballs because of the quasi-crystal structure. However, the characterization of the cluster as an optical material has until now not been achieved. Here we successfully produce icosahedral clusters by assembling silica particles using bulk water-in-oil emulsion droplets and systematically characterize their optical properties. We exploit a water-saturated oil phase to control droplet drying, thereby preparing clusters at room



temperature. In comparison to conventional onion-like supraballs with a similar size, the icosahedral clusters exhibit relatively strong structural colors with weak nonresonant scattering. Simulations prove that the crystalline array inside the icosahedral cluster strengthens the collective specular diffraction. To further improve color saturation, the silica particles constituting the cluster are coated with a thin-film carbon shell. The carbon shell acts as a broad-band absorber and reduces incoherent scattering with long optical paths, resulting in vibrant blue, green, and red colors comparable to inorganic chemical pigments.

■ INTRODUCTION

Colloidal assembly^{1–3} under spherical confinement is interesting both from a fundamental perspective and for a variety of optical applications, including color materials, gas sensors, biosensors, and reflective displays.^{1,4–10} Colloidal particles confined in a constricting droplet (for example, by evaporation) generally organize into an onion-like structure of radially layered face-centered-cubic (FCC) colloidal crystals, often referred to as a supraball.^{1,2} The supraball exhibits wavelength-selective diffraction (that is, structural color), as exhibited by the periodic arrangement of nanoparticles in colloidal crystal films.^{3,11,12} In particular, the color of the structure from the supraball is orientation-independent due to the concentric layered structure of nanoparticles.¹

Supraballs have been prepared by various methods, including electrospray, microfluidics, and inkjet printing, with typical diameters of tens to hundreds of micrometers. $^{13-16}$ Supraballs in this size range may be suitable for applications such as sensors, but not coloring materials; the size of commercially available inorganic coloring particles is on the order of a few micrometers, 17 and commercial reflective displays, such as E-inks, require particles with a diameter of around $10~\mu m$. Despite the great need, there have been only a few reports on the production of supraballs with sizes of a few micrometers. The absence of such studies may be related to the poor color saturation of such small supraballs, which is caused by high defect density and/or a limited number of

layers of particles. The formation of defects is unavoidable, because the layer in which the particles are closely packed is not commensurate with a spherical surface. Furthermore, in the interior of the supraball, colloidal particles may be poorly organized because of the high curvature. The resulting disorder in the particle array causes random scattering as well as incoherent Bragg diffraction, which suppresses structural resonance and consequently deteriorates the optical performance of the supraball. 11,21–24

Recently, Dijkstra, van Blaaderen, and co-workers presented a pioneering study on the formation of icosahedral colloidal clusters for various sizes of particles confined in emulsion drops.⁷ The icosahedral clusters have a minimum free energy configuration for the system containing less than 10^4-10^5 particles. This spherical cluster consists of 20 grains of tetrahedral wedges with deformed FCC crystals; such a structure has no disordered particle array in the interior, which distinguishes it from a typical supraball with a concentric shell. Engel, Vogel, and colleagues have confirmed that the thermodynamic stability of the clusters depends on the number

Received: August 19, 2020 Revised: November 1, 2020 Published: November 16, 2020





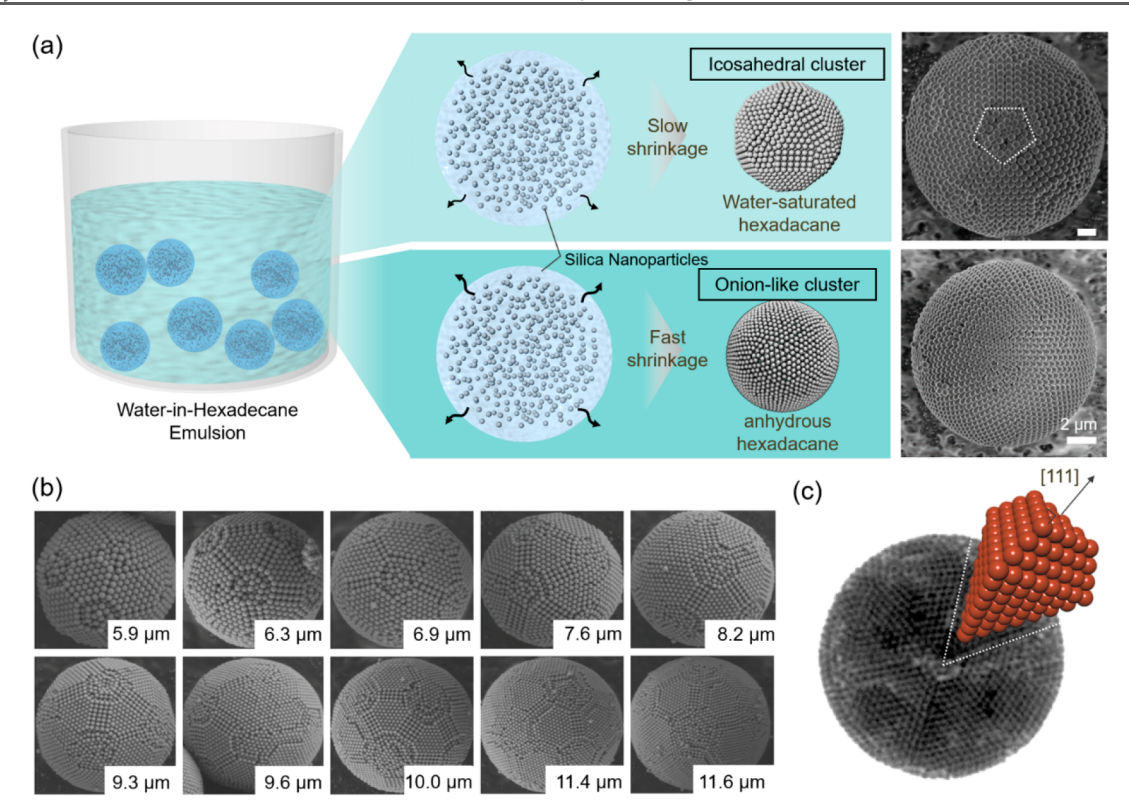


Figure 1. Formation of icosahedral clusters by slow shrinkage of droplets. (a) Schematic showing two different paths for the emulsion droplets to form colloidal clusters, one resulting in icosahedral clusters formed by slow shrinkage in water-saturated hexadecane (top) and the other resulting in onion-like supraballs formed by a fast shrinkage in anhydrous hexadecane (bottom). Scanning electron microscope (SEM) images of the corresponding clusters are shown, where the facet with 5-fold symmetry is denoted with a dotted pentagon in the icosahedral cluster. (b) SEM images of icosahedral clusters with various sizes and colloidal arrangements on the surface. The diameters of the clusters are shown. (c) Confocal microscope image showing the central plane of the icosahedral cluster. The dotted cone represents one tetrahedral grain, and the inset shows the model structure of the grain.

of constituent particles and have shown the existence of "magic numbers" of particles with free energy minima. ^{25,26} In subsequent studies, they identified structural color patterns of the icosahedral cluster that differentiate them from onion-like assemblies. ²⁷ These earlier works come to a consensus that the icosahedral clusters can be prepared in a highly reproducible manner as long as the rate of shrinkage is slow enough to secure the equilibrium state. Moreover, the fully ordered internal structure of the icosahedral cluster enables a significantly improved structural color even for supraballs as small as a few micrometers. Nevertheless, a scalable production scheme of the icosahedral cluster, or its use as a color particle, has not been demonstrated.

Here we demonstrate the scalable production method of icosahedral clusters as well as the preparation of clusters with high color saturation for colorant materials. We use a bulk homogenizing process, rather than a typical microfluidic approach, to form water-in-oil emulsion droplets containing dispersed silica particles. We slowly dry the aqueous droplets using a water-saturated hexadecane medium, which ensures exclusive formation of the icosahedral cluster; in contrast, anhydrous hexadecane results in rapid drying and typical supraballs without icosahedral structures. We image the formation of the supraballs in real time using dual dye labeling under fluorescent confocal microscopy. At the beginning of drying, the silica particles form a concentric shell along the interface of the emulsion droplet, which is maintained for a long time as the droplet continues to dry. The icosahedral

cluster slowly forms in the interior of the droplet when the volume fraction of colloidal particles exceeds about 0.4. At the end of drying, the concentric shell undergoes reconstruction and lattice matches the inner icosahedral cluster. This study experimentally reveals, for the first time, the dynamics of icosahedral cluster formation. In comparison with a typical supraball, the icosahedral cluster exhibits strong structural resonance and weak incoherent scattering, as expected from its high crystallinity. To improve the color saturation, we add a carbon shell, which acts as a broad-band light absorber, to the silica particles. The suppression of background reflection by the carbon shell makes the icosahedral cluster display vivid red, green, and blue colors in air, which is difficult to obtain in conventional supraballs. These carbon-coated icosahedral clusters can be used as practical structural colorants with sizes and color saturations that are comparable to those of chemical pigment particles.

■ RESULTS AND DISCUSSION

To produce icosahedral clusters in a scalable manner, we emulsify an aqueous dispersion of silica particles into hexadecane using a bulk homogenizing process. To include several thousand to tens of thousands of particles in a droplet, we target the diameter of the emulsion droplets to $10-30~\mu m$ by controlling the emulsification conditions and the volume fraction of silica particles, which is set to 5-10~v/v%. The resulting silica-particle-containing aqueous droplets shrink as water slowly dissolves into hexadecane, concentrating the silica

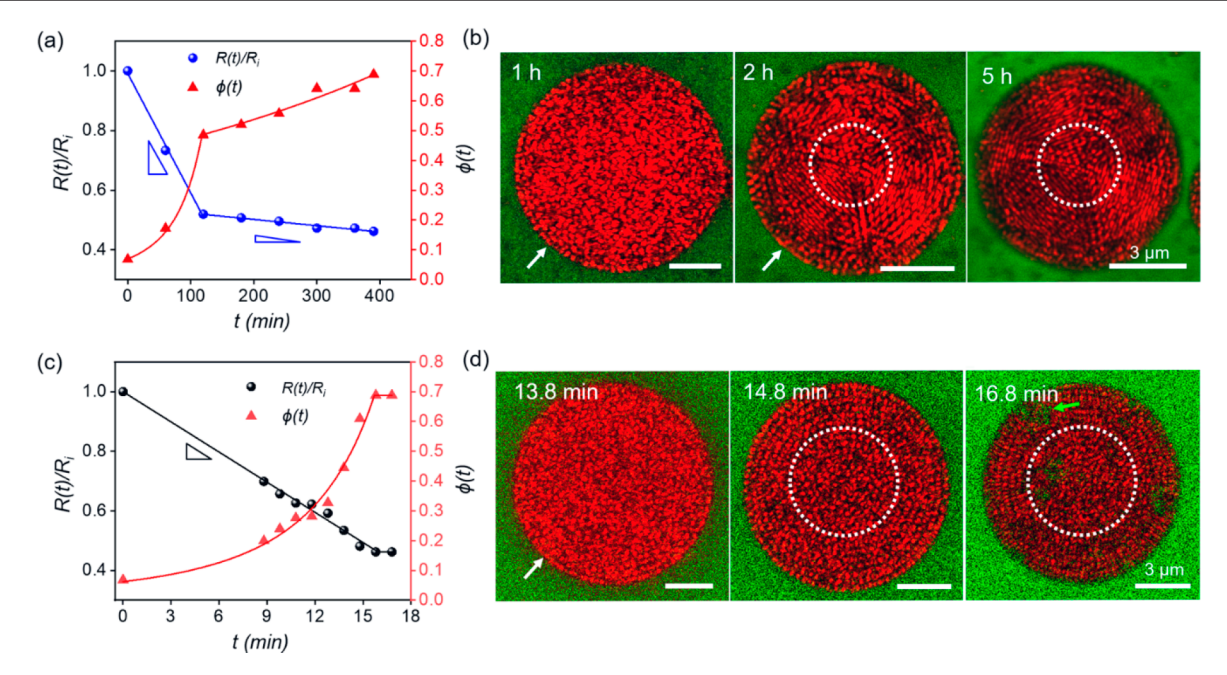


Figure 2. Assembly kinetics for icosahedral clusters and onion-like supraballs. (a) Temporal changes of droplet radius (left *y* axis) and average volume fraction of particles (right *y* axis) for the droplet in water-saturated hexadecane. (b) Series of confocal microscope images showing structural evolution under slow shrinkage, where a red fluorescent dye labels the water and a green fluorescent dye labels the hexadecane. White arrows indicate concentric shells, and dotted circles indicate icosahedral structures. (c, d) Same as in (a, b), but for a droplet in anhydrous hexadecane, which causes rapid shrinkage. A white arrow indicates concentric shells, and dotted circles indicate disordered structures. The green arrow indicates the invasion of the hexadecane into the cluster.

particles. We employ water-saturated hexadecane and anhydrous hexadecane at room temperature to obtain different rates of droplet shrinkage. In water-saturated hexadecane, emulsion droplets shrink slowly over almost 7 h, resulting in icosahedral clusters (top panel of Figure 1a). In contrast, in anhydrous hexadecane, they consolidate in almost 20 min, leaving onion-like supraballs composed of concentric colloidal particle shells (the bottom panel of Figure 1a).

The water-saturated hexadecane suppresses the outflux of water from the droplet to the medium, thereby greatly reducing the shrinkage rate of the droplet. The slow dissolution of water into the water-saturated hexadecane is driven by the Laplace overpressure in the droplet, which also maintains its spherical shape. In comparison to the lowtemperature drying used in previous studies (for example, 5 °C), 26 our protocol does not lower the mobility of the colloidal particles, possibly allowing the formation of icosahedral clusters even under faster drying conditions. Indeed, it took about 7 h to complete the clustering in our experiment, in comparison to days for previous studies. Because the droplets are prepared by bulk emulsification, the resulting clusters are not uniform in size (Figure S1a), but the coefficient of variation (CV) in the diameter of the cluster (d_c) is as small as 16.7%; the average diameter is $d_c = 9.04 \ \mu \text{m}$ (Figure S1b). Icosahedral clusters are formed only when d_c < 14 μ m. That is, icosahedral clusters were formed when the number of particles (N) constituting the cluster is less than N \approx 70000 (when the diameter of the silica particles is $d_p = 299$ nm). In larger clusters, we observe FCC single crystals, consistent with previous results.^{7,27} These FCC single crystals are distinguished by a nearly uniform structural color (that is, reflective color) throughout the entire projection area of the cluster, with some stripes that appear due to stacking faults (Figure S1d).^{6,27} Under typical emulsification conditions, we

identify 77.4% of the clusters as icosahedral, 12.9% as FCC single crystals, and approximately 9.7% as mixed or onion-like supraballs (Figure S1e).

All icosahedral clusters have 20 faces with 5-fold symmetry on the surface regardless of their size, as each is a Mackay icosahedron whose outer region is truncated to accommodate the spherical droplet. The specific particle arrangement on the quasi-spherical surface depends on the size of the cluster (Figure 1b). For a cluster composed of approximately $N \approx$ 5290 particles ($d_c = 5.9 \mu \text{m}$, $\hat{d}_p = 299 \text{ nm}$), the surface comprises only pentagonal and hexagonal patches, like a soccer ball; the hexagonal patches consist of hexagonal arrays of particles. As the number of particles increases, rectangular patches, composed of a square array of particles corresponding to FCC {100} planes, appear. Their width increases as the hexagonal patches gradually turn into triangular patches (Figure 1b). The rectangular patches contain three strings of particles for $N \approx 6440-8460$ ($d_c \approx 6.3-6.9 \mu m$), four strings for $N \approx 11300-14200$ ($d_c \approx 7.6-8.2 \mu m$), and five strings for $N \approx 20700~(d_{\rm c} \approx 9.3~\mu{\rm m})$, which is consistent with previous reports. ^{7,26} For clusters with $d_c > 9.3 \mu m$, there is a variation of the number of the colloidal strings in rectangular patches. This structural evolution on the surface arrangement is naturally caused by the different degrees of truncation needed to accommodate the curvature.7,

We observe the internal structure of an icosahedral cluster with a confocal microscope (Figure 1c) by filling its interstitial voids with a dye-dissolved mixture of water and glycerol (the volume ratio of water and glycerol is 1:4, whose refractive index matches the silica particles to minimize scattering). We see that tetrahedral grains are twinned with their neighbors, and no disordered structure is formed even in the center. Each tetrahedral grain has a slightly deformed FCC lattice whose [111] direction is radially aligned (see model structure in

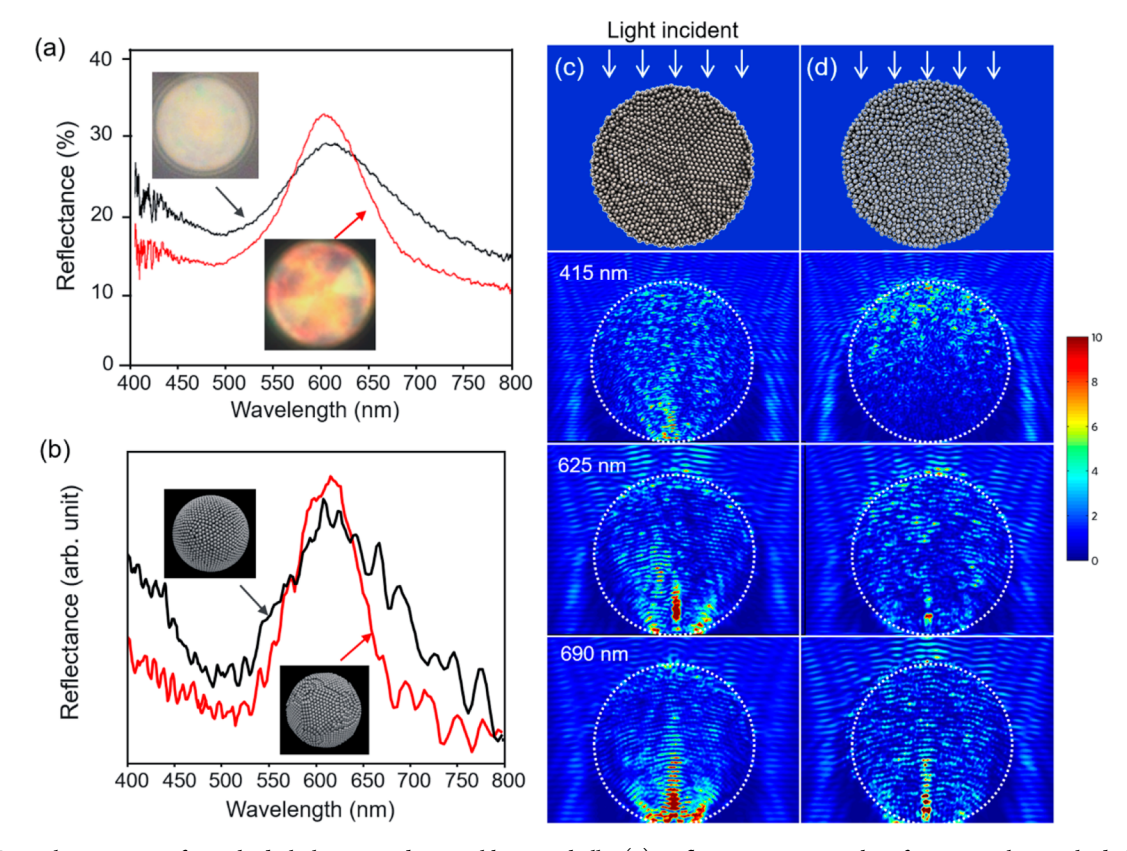


Figure 3. Optical properties of icosahedral clusters and onion-like supraballs. (a) Reflectance spectra taken from a single icosahedral cluster and onion-like supraball. Insets are optical microscope images of the corresponding clusters. (b) Reflectance spectra for model structures (insets) calculated using a FDTD simulation. (c, d) Cross-sectional views of model structures used in the FDTD simulations (top; see also Figure S6) and calculated electric-field distributions at 415 nm wavelength (second from top), 620 nm (third from top), and 690 nm (bottom panels) for the icosahedral cluster (c) and supraball (d).

Figure 1c). ²⁶ This structure, which is clearly distinguished from onion-like supraballs composed of concentric shells and less ordered interiors, ^{1,11} creates the possibility of enhanced optical performance.

To study the influence of the droplet shrinkage rate on the assembly behavior of particles, we monitor the droplets during the entire process of shrinkage. Over approximately t=2 h, the radius of a droplet, R, in the water-saturated hexadecane linearly decreases to half of the initial value, R_i . Afterward it linearly decreases but with a smaller slope (blue curves in Figure 2a); the linearity implies a constant rate of water transfer through a unit surface area of droplet to the surrounding medium. The shrinkage increases the volume fraction of silica particles in the droplet from $\phi_i = 0.068$ to $\phi = 0.485$ at t=2 h and $\phi = 0.688$ at t=6.5 h (red curves in Figure 2a):

$$\phi(t) = \phi_{\rm i} \left(\frac{R_{\rm i}}{R(t)}\right)^3 \tag{1}$$

We attribute the sudden reduction of the rates of shrinkage observed at t=2 h and $\phi=0.485$ to the water solvating the silica particles, which requires a strong driving potential to be quickly removed; we estimate the thickness of the solvation layer at $\phi=0.485$ to be 31 nm for silica particles with $d_{\rm p}=500$ nm by assuming that the colloidal array has the structure of a non-close-packed Mackay icosahedron.

We also monitor the colloidal arrangement in real time using a confocal microscope (Figure 2b) by dissolving a red fluorescent dye in water and a green fluorescent dye in hexadecane; by using two dyes, we can observe the drying of water as well as the arrangement of particles. We find that the particles form a monolayered shell along the interface of the droplet in t=1 h ($\phi=0.172$), while they maintain a disordered array in the interior (left panel in Figure 2b). We estimate the Péclet number (Pé) of the system, the ratio of the convection rate of the droplet surface to the diffusion rate of the particles, to be 0.00474:

$$P\acute{e} = \frac{Ru}{D} \tag{2}$$

where the diffusivity of particles, D, is $9.81 \times 10^{-13} \, \mathrm{m}^2/\mathrm{s}$, on the basis of the Stokes–Einstein relation for $d_\mathrm{p} = 500 \, \mathrm{nm}$, the rate of shrinkage, u, is $u = \mathrm{d}R/\mathrm{d}t = 5.58 \times 10^{-10} \, \mathrm{m/s}$, on the basis of the reduction in size for the first 2 h, and $R_\mathrm{i} = 8.35 \, \mu\mathrm{m}$. The small Péclet number shows that diffusion dominates convection, which helps the droplet to remain in a quasiequilibrium state during shrinkage.

Nevertheless, the particles form a colloidal shell along the interface in t=1 h, which we attribute to the restricted mobility of particles in the presence of the nearly immobile interface. The colloidal particles in the interior form a structure with icosahedral symmetry in t=2 h, whereas the shell grows to have three to four layers and persists ($\phi=0.485$, the middle panel in Figure 2b). Afterward, there are no significant changes to the interior particle arrangement, but the outer concentric shells disappear, and the particles rearrange to complete the formation of an icosahedral cluster in 5 h (right panel of Figure

2b). At 5 h we observe the formation of planar faces on the surface in magnified images (Figure S2). The rearrangement of concentric shells takes 3 h, which is 60% of the entire shrinkage duration. The hexadecane invades the interstitial voids of the cluster at 6 h, indicating that the water is almost entirely removed (Figure S3).

Overall, the process of icosahedral cluster formation, which has never been directly observed, is consistent with event-driven simulations for hard spheres. In our experimental system, however, interparticle repulsion lowers the volume fraction of particles at the onset of crystallization to approximately $\phi = 0.4$, whereas hard spheres crystallize at $\phi = 0.49$. Also, our observations show slow and gradual surface rearrangement from quasi-solid concentric shells accompanied by a 10-fold reduction in shrinkage rate. In contrast, hard spheres in the concentric shells remain mobile and show relatively fast rearrangement in simulations. We attribute the difference to the interparticle repulsion, which endows a relatively high energy barrier for rearrangement of the particles.

Droplets in anhydrous hexadecane shrink rapidly in comparison with those in water-saturated hexadecane. At the moment when we first observe the droplets, they are already shrunken owing to the fast dissolution of water. The radius of the droplet linearly decreases over the incubation time for the entire process after observation (Figure 2c). There is no change in the rate of shrinkage because the volume of hexadecane is large, and hence the driving potential for the dissolution of water remains high during the entire process.

By assuming that linearity is conserved before observation and that the final volume fraction of particles is $\phi = 0.688$ (the limiting value for a Mackay icosahedron²⁶), we can estimate the initial radius of the droplet and the interval between droplet formation and the first observation from the final radius of the cluster (Figure 2c). We thus estimate the initial radius to be R_i = 11.7 μm and the interval to be 8.8 min. The estimated Pé value is 0.0781 ($u = dR/dt = 6.57 \times 10^{-9}$ m/s), indicating that diffusion dominates convection even under rapid drying. Nevertheless, icosahedral order is not achieved because heterogeneous nucleation on the interface at the early stage dictates the overall crystallization process. The fast shrinkage and consolidation kinetically arrest the concentric shells and do not allow rearrangement of particles. As shown in the confocal microscope images, the particles form a monolayered shell along the interface in 13.8 min (left panel of Figure 2d), and the shell gets thicker with time as the crystal grows radially toward the center of the droplet (middle panel of Figure 2d). Each shell is predominantly composed of a hexagonal array of particles with many defects due to the curvature (inset of Figure 1a). The radial direction corresponds to the [111] direction of the FCC lattice. 1,11,28 The water is depleted in 16.8 min, as confirmed by the invasion of the hexadecane into the final cluster. At this point, the particles in the core remain disordered (right panel of Figure 2d).

We carefully investigate and compare the optical property of two distinct structures—the icosahedral cluster and onion-like supraball—with reflectance measurements (Figure 3a). The spectra are acquired from a single cluster using a microscope with a 50× objective lens and a numerical aperture (NA) of 0.8. Both structures show a reflectance peak at 615 nm originating from structural resonance. The peak position, λ_{max} is consistent with the Bragg equation for {111} planes of a slightly deformed FCC lattice:

$$\lambda_{\text{max}} = 2\alpha d_{111} (n_{\text{eff}}^2 - \cos \theta^2)^{1/2}$$
 (3)

where d_{111} is the spacing between neighboring {111} planes of a perfect FCC structure and $n_{\rm eff}$ is the effective refractive index approximated from the average refractive index of silica and air weighted by their volume fractions; $d_{111} = 244$ nm for $d_{\rm p} = 299$ nm and $n_{\rm eff} \approx 1.306$ for $\phi = 0.688$ for the large Mackay icosahedron. The correction factor, α , is the ratio of the spacing between {111} planes of the deformed FCC structure in the Mackay icosahedron to that of a perfect FCC structure, which is 0.97325 (Figure S4). Equation 3 gives $\lambda_{\rm max} = 620$ nm for normal incidence, $\theta = 90^{\circ}$.

Thus, the structural resonance occurs at the {111} planes of a slightly deformed FCC lattice because the [111] direction is radially aligned for both structures. Although the [111] direction is aligned exactly vertically only when one of the tetrahedral grains is vertical for the icosahedral structure, the use of a lens with an NA value of 0.8 makes the incident light converge onto the quasi-spherical surface, reflecting light at the resonant wavelength for an almost normal reflection, not strongly depending on the orientation of the cluster (Figure S5). The clusters show color patterns depending on the orientation of the tetrahedral grains.²⁷ For example, the cluster shows a bow-tie-like pattern for the specific orientation shown in the inset of Figure 3a. In contrast, the onion-like supraball shows a more uniform color with the brightest spot on the top irrespective of the orientation since the structure is isotropic (inset of Figure 3a).

It is noteworthy that the icosahedral cluster shows a higher reflected intensity at the resonant wavelength and a lower intensity at off-resonant wavelengths in comparison to the supraball (Figure 3a); this spectral feature is important to develop structural colors with high saturation. To study the origin of this spectral feature, we first construct the model structure by a molecular dynamics (MD) simulation (Figure S6) and then obtain the optical spectrum for this structure by a finite-difference time-domain (FDTD) simulation. For the MD simulation, we randomly arrange particles in a spherical cavity and reduce the cavity at a constant rate to form an assembly. The potential between particles is approximated as the Weeks-Chandler-Anderson (WCA) potential,²⁹ and the potential between the nanoparticle and the cavity surface is approximated as a harmonic potential. We obtain structures that simulate the icosahedral cluster and the supraball by using different rates of reduction in cavity size, as in the experiment (Figure S6). The FDTD simulation shows a peak of 620 nm in the reflection spectrum from each model cluster (Figure 3b). The intensity at the resonant wavelength for the icosahedral cluster is slightly higher and that at the off-resonant wavelength is lower, which is consistent with the experimental result.

To further scrutinize the origin of enhanced color saturation that the icosahedral cluster exhibits, we visualize the electric-field distribution at three different wavelengths of 415, 620, and 690 nm (Figure 3c,d). At 620 nm, strong collective diffraction is observed over the upper hemisphere of the cluster in comparison with the supraball (third panels from the top). The large transmitted field at the bottom is caused by lensing of the incident beam at the upper surface of the cluster. These results indicates that random scattering by particles is suppressed in the icosahedral cluster because it does not contain a disordered array. ^{30–32} At 415 nm, the optical responses for the cluster and supraball are markedly different. In the supraball, strong scattering is observed over the upper

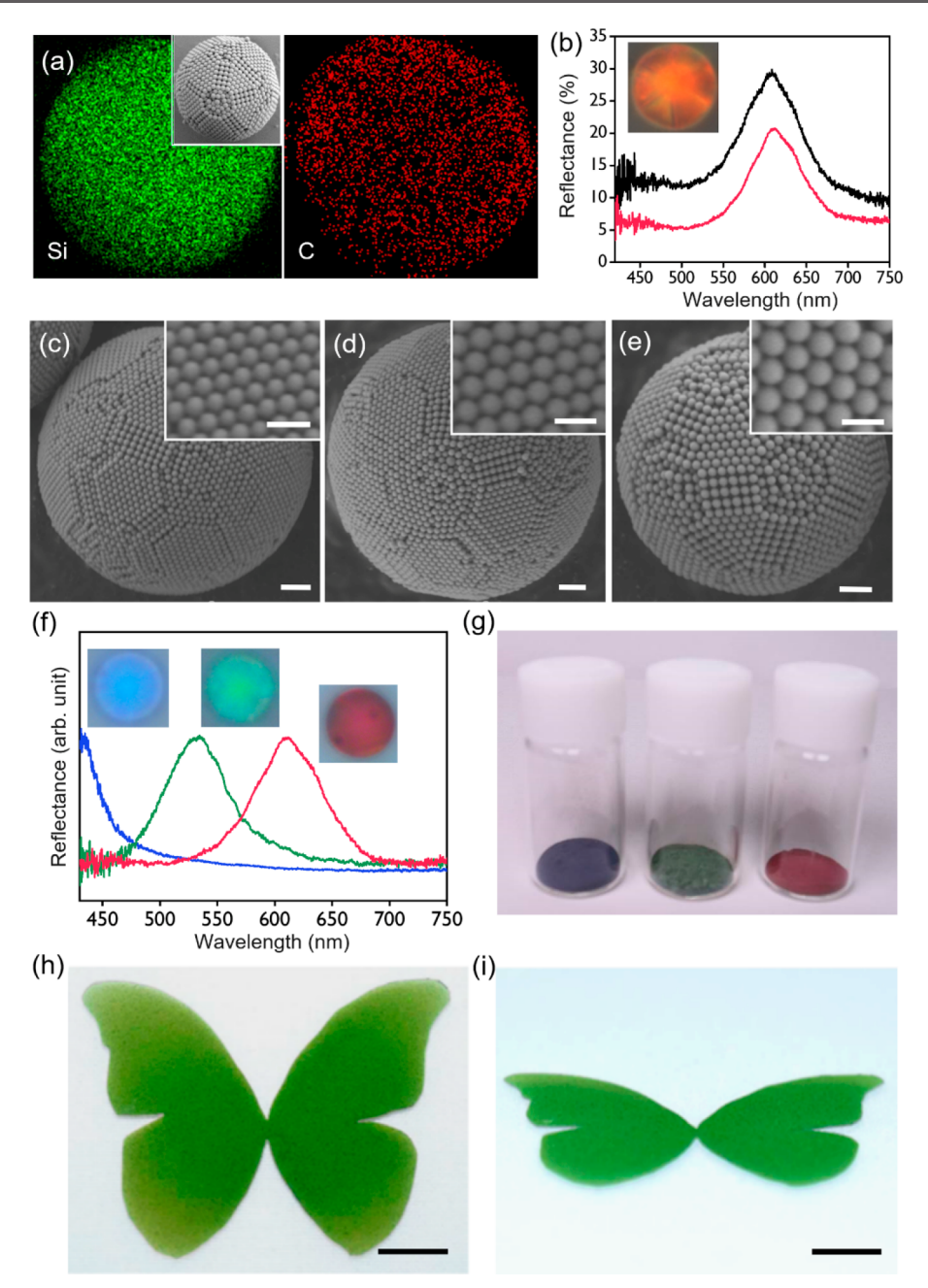


Figure 4. Structural colorants with high saturation. (a) Elemental mapping images of silicon (left panel) and carbon (right panel) for the icosahedral cluster shown in the inset SEM image. (b) Reflection spectra of icosahedral clusters without (black curve) and with a carbon coating (red curve). The inset is an optical microscope image of a carbon-coated icosahedral cluster. (c–e) SEM images of carbon-coated icosahedral clusters composed of silica particles with diameters of (c) 190 nm, (d) 235 nm, and (e) 275 nm (scale bar: 1 μm). The insets are magnified views of a facet of a hexagonal array. (f) Reflection spectra and (g) photographs of the icosahedral clusters in (c–e). (h, i) Photographs of a butterfly pattern formed by spraying the carbon-coated icosahedral clusters on paper taken at two different angles (scale bar: 5 mm).

hemisphere (second panel of Figure 3d), resulting in high intensity in the spectrum (Figure 3b); this result is consistent with the results of analytical calculations on the cavity resonance of each particle reported by Magkiriadou and coworkers.³³ In contrast, the scattering is much reduced in the icosahedral particles and the incident light is refracted, propagating through the cluster (second panel of Figure 3c). As a result, the reflection is weak at that wavelength (Figure 3b). At 690 nm, both the cluster and supraball show strong transmission because of the long attenuation length at this wavelength (bottom panels of Figure 3c,d). Nevertheless, there is a clear contrast in the electric-field distribution: the

icosahedral cluster behaves more like a lens, whereas the supraball behaves more as a collection of random scatterers. In summary, the long-range order in the absence of defects for the icosahedral cluster builds up strong structural resonance through Bragg diffraction and suppresses incoherent random scattering, thereby improving color saturation. Indeed, a powder sample of the icosahedral clusters is a clear red, whereas that of the supraballs appears white (Figure S7a,b).

The color saturation of colloidal structures can be enhanced by incorporating light-absorbing additives. For example, Stein and co-workers added carbon nanoparticles to colloidal crystals composed of polymer particles.³⁴ Seki and co-workers used

carbon nanoparticles in conventional supraballs.³⁵ Kim and coworkers used polydopamine nanoparticles in non-close-packed colloidal arrays in the form of films or balls. 36,37 Aizenberg and co-workers incorporated gold nanoparticles in supraballs to absorb specific wavelengths of light. However, the presence of the additives in the droplets may influence the interparticle potential and assembly behavior of particles, possibly perturbing the formation of icosahedral clusters. Therefore, we introduce a light-absorbing component, carbon, through a post-treatment process. We dilute phenol-formaldehyde resol, a precursor of carbon, in ethanol at 80 v/v% and then drop it onto a powder of the clusters. After the residue is washed with ethanol, we treat the sample at 100 $^{\circ}\text{C}$ for 24 h to cross-link the resol. The resol is then carbonized by treatment at 700 °C under an argon atmosphere for 2 h. As a result, each silica particle in the cluster is coated by a carbon shell. The carbon is uniformly distributed on the entire surface of the cluster without deteriorating the structure (Figure 4a). The carbon shell is formed on the surface of silica particles with a thickness of a few nanometers. According to an X-ray photoelectron spectroscopy (XPS) analysis (Figure S8), the carbon makes up about 2-3 wt % of the clusters.

The carbon coating reduces the reflected intensity over the entire visible range without changing the peak position (Figure 4b). The reduction in the intensity at short wavelengths is 30–40% larger than at long wavelengths. Although the reflection at the resonant wavelength is also reduced from 30% to 21%, the reduction of the scattering at off-resonant wavelengths toward zero enhances the color saturation remarkably, as can be seen in optical microscope images of a single cluster (inset of Figure 4b) and photographs of a powder (Figure S7c). It is noteworthy that a vibrant red can be seen in clusters with diameters of several micrometers. It is much more challenging to develop structural red than it is to make blue and green because the larger particles that are responsible for the resonance at long wavelengths scatter the light more strongly off-resonance, leading to tinted or pale red.³³

The structural color of the icosahedral clusters can be tuned by adjusting the size of the silica particles. We find that icosahedral clusters are formed regardless of the size of silica particles at least in the range of $d_{\rm p}=205-299$ nm (Figure 4c–e). The clusters composed of silica particles with $d_{\rm p}=205$, 255, and 299 nm are blue, green, and red, respectively (Figure 4f,g). Equation 3 predicts resonant wavelengths of $\lambda_{\rm max}=426$, 529, and 620 nm, which are close to the reflectance peaks of 425, 530, and 615 nm (Figure 4f); for $d_{\rm p}=205$ nm the peak cannot be clearly seen within the range of the measurement. The color saturation of the powders is comparable to that of commercially available chemical pigments, even with a white background. Also, the powders show a consistent color regardless of the viewing angle under diffuse illumination because the clusters have a quasi-isotropic structure (Figure S9).

We prepare a butterfly pattern by spraying the green clusters through a mask onto paper (Figure 4h,i. Even though the substrate is white, the pattern displays a vivid green color, which remains unchanged with viewing angle under ambient light. To compare the optical properties of the icosahedral clusters to those of the onion-like supraballs, we created a similar system from onion-like supraballs by following the same carbonization protocol for the same size of silica particles as in the icosahedral clusters (Figure S10). The powder of the carbon-coated supraballs is purple and not red, indicating that

scattering at short wavelengths is not suppressed even in the presence of the carbon. We attribute the absence of suppression to strong scattering from the disordered interior.

CONCLUSION

In this study, we produced icosahedral clusters by slowly shrinking particle-laden water droplets in water-saturated oil. Because the emulsion droplets are prepared by bulk emulsification and the room-temperature process reduces the time scale for the shrinkage, the protocol we designed is scalable and reproducible, and it can serve as a practical way to create icosahedral clusters in large quantities. The time scale might be further reduced to increase the throughput because most of the time is spent on the rearrangement of concentric shells with low mobility, and a few layers of concentric shells should have no significant effects on the structural color. Importantly, the icosahedral clusters show superior optical properties in comparison to typical onion-like supraballs because they have no disordered internal structures. Moreover, adding a carbon coating through post-treatment further improves the saturation of structural colors, resulting in vibrant structural colors even for red as well as blue and green. These carbon-coated clusters can serve as practical structural colorants because their optical performance and size are comparable to those of commercial chemical pigments.

■ EXPERIMENTAL SECTION

Fabrication of Icosahedral Clusters and Supraballs. We synthesized colloidal silica by the Stober method. We emulsified an aqueous dispersion of 5–10 v/v% silica particles into hexadecane containing 3 w/w% surfactant of poly(isobutylene)succinic anhydride–polyethylene glycol (Sigma-Aldrich) using a homogenizer (IKA, T-18) at 3000 rpm. For slow shrinkage of droplets, we used hexadecane saturated with water. The water-saturated hexadecane was prepared by incubating 1 mL of hexadecane with 1 μ L of water at 50 °C. For fast shrinkage, we used anhydrous hexadecane. The clusters were washed several times with hexane and dried to obtain a powder. Any organic residues were removed by heat treatment at 500 °C in air for 30 min.

Carbon Coating. Phenol-formaldehyde resol was used as a carbon precursor. This resol was obtained by reacting 6.5 mmol of phenol and 36 w/w% of formaldehyde solution in 20 w/w% NaOH solution at 70 °C for 1 h. Afterward, a 0.6 M HCl solution was added to the reaction solution. The phenol-formaldehyde resol diluted in ethanol at 80 v/v% was dropped onto a powder of the clusters. The residue was washed with ethanol several times. The sample was treated at 100 °C for 24 h to cross-link the resol. The resol was carbonized by treatment under an argon atmosphere at 700 °C for 2 h.

Characterizations. The surface morphology and energy-dispersive X-ray (EDX) elemental mapping were measured by an SEM (SUPRA 55VP, Carl Zeiss). Optical properties were determined with an upright optical microscope in reflection mode (Nikon, ECLIPSE LV100) using a $50 \times$ objective (Nikon, LU Plan Fluor, NA = 0.8) and a digital camera (Nikon DS-5Mc). The reflection spectra were measured using a fiber optic spectrometer (Ocean Optics Inc., HR 2000+, QP600-2-UV/vis) coupled to the optical microscope. All spectra were normalized using a reference measured on a sample-free Si wafer substrate. The assembly behavior of particles in droplets and the internal structure of clusters were observed using a confocal laser scanning microscope (Leica DM IRBE microscope, Leica Microsystems GmbH, Wetzlar, Germany). For real-time observation of particles in droplets, the water phase was labeled with a red dye, 4-[4-[4-(dimethylamino)phenyl]-1,3-butadienyl]-1-ethylpyridinium perchlorate, and the hexadecane was labeled with a green dye, 2dimethylaminonaphthalene-6-sulfonyl chloride. For the observation of internal structure, clusters were suspended in a mixture of water and

glycerol in a 1:4 volume ratio containing a dye of rhodamine 6G to match the refractive index. X-ray photoelectron spectroscopy (XPS, Thermo Fisher Scientific, ESCALAB 250 XPS System) analysis using a monochromated Al K α X-ray source ($h_{\rm v}=1486.6~{\rm eV}$) at a chamber pressure of 1 \times 10⁻¹⁰ Torr was performed for elemental analysis.

Finite-Difference Time-Domain (FDTD) Simulation. Optical simulations were performed using FDTD Solutions (v. 8.17.1102, Lumerical Solutions, Canada). First, the coordinates of particles that make up the icosahedral cluster and supraball were extracted from MD simulations. Using the coordinates, we reconstructed the structures for the FDTD simulation, where the particles were set to lie on the xy plane and the position of the particle at the plane was set to (x, y, z) = (0, 0, 0). We projected polarized plane waves of various wavelengths from 400 to 800 nm perpendicular to the top surface of the cluster. The size of the simulation volume was set to $15 \times 15 \times 25$ μ m³ (width \times length \times height). We applied PML boundary conditions. Complex refractive indices for SiO₂ particles were imported from Palik's Handbook of Optical Constants. The reflected or scattered spectrum was recorded by a power monitor in the xy plane located above the plane wave source.

ASSOCIATED CONTENT

5 Supporting Information

The Supporting Information is available free of charge at https://pubs.acs.org/doi/10.1021/acs.chemmater.0c03391.

Size distribution of the clusters, confocal microscopy images in real time, analysis of FCC planar spacing and light reflection for clusters, MD simulation for the model structure, cross-sectional SEM images of supraballs and clusters, change in color saturation by carbon coating, TEM image of the coated carbon layer, angular independence of structural colors, and color comparison of carbon-coated supraballs and clusters (PDF)

AUTHOR INFORMATION

Corresponding Authors

Hyerim Hwang — Harvard John A. Paulson School of Engineering and Applied Sciences, Harvard University, Cambridge, Massachusetts 02138, United States; orcid.org/0000-0001-8098-6030;

Email: hyerimhwang@fas.harvard.edu

Vinothan N. Manoharan — Harvard John A. Paulson School of Engineering and Applied Sciences and Department of Physics, Harvard University, Cambridge, Massachusetts 02138, United States; ● orcid.org/0000-0003-0370-6095; Email: vnm@seas.harvard.edu

Jun Hyuk Moon — Department of Chemical and Biomolecular Engineering, Institute of Emergent Materials, Sogang University, Seoul 04107, Republic of Korea; oocid.org/ 0000-0002-4776-3115; Email: junhyuk@sogang.ac.kr

Authors

Cheolho Kim — Department of Chemical and Biomolecular Engineering, Sogang University, Seoul 04107, Republic of Korea

Kinam Jung – Department of Mechanical Engineering, Hannam University, Daejeon 34430, Republic of Korea

Ji Woong Yu — School of Chemical and Biological Engineering, Institute of Chemical Processes, Seoul National University, Seoul 08826, Republic of Korea

Sanghyuk Park – Department of Chemical and Biomolecular Engineering, Korea Advanced Institute of Science and Technology (KAIST), Daejeon 34141, Republic of Korea Shin-Hyun Kim — Department of Chemical and Biomolecular Engineering, Korea Advanced Institute of Science and Technology (KAIST), Daejeon 34141, Republic of Korea; orcid.org/0000-0003-4095-5779

Won Bo Lee — School of Chemical and Biological Engineering, Institute of Chemical Processes, Seoul National University, Seoul 08826, Republic of Korea; orcid.org/0000-0001-7801-083X

Complete contact information is available at: https://pubs.acs.org/10.1021/acs.chemmater.0c03391

Author Contributions

 $^{\nabla}$ C.K., K.J., and J. W. Y. contributed equally.

Notes

The authors declare no competing financial interest.

ACKNOWLEDGMENTS

This work was supported by National Research Foundation of Korea grant numbers 2019R1A2C2009123, 2019R1A4A1027627, 2018M3A7B8060189, 2017R1C1B5074916 and by the Harvard University Materials Research Science and Engineering Center under National Science Foundation grant number DMR-2011754.

REFERENCES

- (1) Zhao, Y.; Shang, L.; Cheng, Y.; Gu, Z. Spherical Colloidal Photonic Crystals. *Acc. Chem. Res.* **2014**, *47*, 3632–3642.
- (2) Li, B.; Zhou, D.; Han, Y. Assembly and phase transitions of colloidal crystals. *Nat. Rev. Mater.* **2016**, *1*, 1.
- (3) von Freymann, G.; Kitaev, V.; Lotschz, B. V.; Ozin, G. A. Bottom-up assembly of photonic crystals. *Chem. Soc. Rev.* **2013**, 42, 2528–2554.
- (4) Irvine, W. T. M.; Vitelli, V.; Chaikin, P. M. Pleats in crystals on curved surfaces. *Nature* **2010**, 468, 947–951.
- (5) Meng, G. N.; Paulose, J.; Nelson, D. R.; Manoharan, V. N. Elastic Instability of a Crystal Growing on a Curved Surface. *Science* **2014**, 343, 634–637.
- (6) Choi, T. M.; Lee, G. H.; Kim, Y. S.; Park, J. G.; Hwang, H.; Kim, S. H. Photonic Microcapsules Containing Single-Crystal Colloidal Arrays with Optical Anisotropy. *Adv. Mater.* **2019**, *31*, 1900693.
- (7) de Nijs, B.; Dussi, S.; Smallenburg, F.; Meeldijk, J. D.; Groenendijk, D. J.; Filion, L.; Imhof, A.; van Blaaderen, A.; Dijkstra, M. Entropy-driven formation of large icosahedral colloidal clusters by spherical confinement. *Nat. Mater.* **2015**, *14*, 56–60.
- (8) Kim, S.-H.; Jeon, S.-J.; Yang, S.-M. Optofluidic encapsulation of crystalline colloidal arrays into spherical membrane. *J. Am. Chem. Soc.* **2008**, 130, 6040–6046.
- (9) Choi, T. M.; Je, K.; Park, J.-G.; Lee, G. H.; Kim, S.-H. Photonic Capsule Sensors with Built-In Colloidal Crystallites. *Adv. Mater.* **2018**, 30, 1803387.
- (10) Zhao, Y.; Zhao, X.; Sun, C.; Li, J.; Zhu, R.; Gu, Z. Encoded Silica Colloidal Crystal Beads as Supports for Potential Multiplex Immunoassay. *Anal. Chem.* **2008**, *80*, 1598–1605.
- (11) Vogel, N.; Utech, S.; England, G. T.; Shirman, T.; Phillips, K. R.; Koay, N.; Burgess, I. B.; Kolle, M.; Weitz, D. A.; Aizenberg, J. Color from hierarchy: Diverse optical properties of micron-sized spherical colloidal assemblies. *Proc. Natl. Acad. Sci. U. S. A.* **2015**, *112*, 10845–10850.
- (12) Wong, S.; Kitaev, V.; Ozin, G. A. Colloidal crystal films: advances in universality and perfection. *J. Am. Chem. Soc.* **2003**, *125*, 15589–15598.
- (13) Hu, J.; Zhao, X.-W.; Zhao, Y.-J.; Li, J.; Xu, W.-Y.; Wen, Z.-Y.; Xu, M.; Gu, Z.-Z. Photonic crystal hydrogel beads used for multiplex biomolecular detection. *J. Mater. Chem.* **2009**, *19*, 5730–5736.

- (14) Shang, L.; Shangguan, F.; Cheng, Y.; Lu, J.; Xie, Z.; Zhao, Y.; Gu, Z. Microfluidic generation of magnetoresponsive Janus photonic crystal particles. *Nanoscale* **2013**, *5*, 9553–9557.
- (15) Takeoka, Y.; Yoshioka, S.; Teshima, M.; Takano, A.; Harun-Ur-Rashid, M.; Seki, T. Structurally Coloured Secondary Particles Composed of Black and White Colloidal Particles. *Sci. Rep.* **2013**, *3*, 2371.
- (16) Zhao, Y.; Zhao, X.; Hu, J.; Xu, M.; Zhao, W.; Sun, L.; Zhu, C.; Xu, H.; Gu, Z. Encoded Porous Beads for Label-Free Multiplex Detection of Tumor Markers. *Adv. Mater.* **2009**, *21*, 569–572.
- (17) Bittler, K.; Ostertag, W. Developments in the Field of Inorganic Pigments. *Angew. Chem., Int. Ed. Engl.* **1980**, *19*, 190–196.
- (18) Comiskey, B.; Albert, J. D.; Yoshizawa, H.; Jacobson, J. An electrophoretic ink for all-printed reflective electronic displays. *Nature* **1998**, 394, 253–255.
- (19) Marshall, K.; Kimball, E.; McNamara, S.; Kosc, T.; Trajkovska-Petkoska, A.; Jacobs, S. Electro-optical behavior of polymer cholesteric liquid crystal flake/fluid suspensions in a microencapsulation matrix; SPIE: Bellingham, WA, 2004; Vol. 5518, pp 170–181.
- (20) Bausch, A. R.; Bowick, M. J.; Cacciuto, A.; Dinsmore, A. D.; Hsu, M. F.; Nelson, D. R.; Nikolaides, M. G.; Travesset, A.; Weitz, D. A. Grain boundary scars and spherical crystallography. *Science* **2003**, 299, 1716–1718.
- (21) Ballato, J. Tailoring visible photonic bandgaps through microstructural order and coupled material effects in SiO2 colloidal crystals. *J. Opt. Soc. Am. B* **2000**, *17*, 219–225.
- (22) Rojas-Ochoa, L. F.; Mendez-Alcaraz, J. M.; Saenz, J. J.; Schurtenberger, P.; Scheffold, F. Photonic properties of strongly correlated colloidal liquids. *Phys. Rev. Lett.* **2004**, *93*, 93.
- (23) Pursiainen, O. L. J.; Baumberg, J. J.; Winkler, H.; Viel, B.; Spahn, P.; Ruhl, T. Nanoparticle-tuned structural color from polymer opals. *Opt. Express* **2007**, *15*, 9553–9561.
- (24) Liew, S. F.; Yang, J.-K.; Noh, H.; Schreck, C. F.; Dufresne, E. R.; O'Hern, C. S.; Cao, H. Photonic band gaps in three-dimensional network structures with short-range order. *Phys. Rev. A: At., Mol., Opt. Phys.* **2011**, *84*, 063818.
- (25) Wang, J.; Mbah, C. F.; Przybilla, T.; Englisch, S.; Spiecker, E.; Engel, M.; Vogel, N. Free Energy Landscape of Colloidal Clusters in Spherical Confinement. *ACS Nano* **2019**, *13*, 9005–9015.
- (26) Wang, J.; Mbah, C. F.; Przybilla, T.; Zubiri, B. A.; Spiecker, E.; Engel, M.; Vogel, N. Magic number colloidal clusters as minimum free energy structures. *Nat. Commun.* **2018**, *9*, 5259.
- (27) Wang, J.; Sultan, U.; Goerlitzer, E. S. A.; Mbah, C. F.; Engel, M.; Vogel, N. Structural Color of Colloidal Clusters as a Tool to Investigate Structure and Dynamics. *Adv. Funct. Mater.* **2020**, *30*, 1907730.
- (28) Zhao, Y.; Cheng, Y.; Shang, L.; Wang, J.; Xie, Z.; Gu, Z. Microfluidic Synthesis of Barcode Particles for Multiplex Assays. *Small* **2015**, *11*, 151–174.
- (29) Toxvaerd, S.; Dyre, J. C. Role of the first coordination shell in determining the equilibrium structure and dynamics of simple liquids. *J. Chem. Phys.* **2011**, *135*, 134501.
- (30) Prum, R. O.; Torres, R. H.; Williamson, S.; Dyck, J. Coherent light scattering by blue feather barbs. *Nature* **1998**, *396*, 28–29.
- (31) Tikhonov, A.; Coalson, R. D.; Asher, S. A. Light diffraction from colloidal crystals with low dielectric constant modulation: Simulations using single-scattering theory. *Phys. Rev. B: Condens. Matter Mater. Phys.* **2008**, 77, 235404.
- (32) Vos, W. L.; Sprik, R.; Vanblaaderen, A.; Imhof, A.; Lagendijk, A.; Wegdam, G. H. Strong effects of photonic band structures on the diffraction of colloidal crystals. *Phys. Rev. B: Condens. Matter Mater. Phys.* 1996, 53, 16231–16235.
- (33) Magkiriadou, S.; Park, J. G.; Kim, Y. S.; Manoharan, V. N. Absence of red structural color in photonic glasses, bird feathers, and certain beetles. *Phys. Rev. E* **2014**, *90*, 062302.
- (34) Aguirre, C. I.; Reguera, E.; Stein, A. Colloidal Photonic Crystal Pigments with Low Angle Dependence. *ACS Appl. Mater. Interfaces* **2010**, *2*, 3257–3262.

- (35) Takeoka, Y.; Yoshioka, S.; Takano, A.; Arai, S.; Nueangnoraj, K.; Nishihara, H.; Teshima, M.; Ohtsuka, Y.; Seki, T. Production of Colored Pigments with Amorphous Arrays of Black and White Colloidal Particles. *Angew. Chem., Int. Ed.* **2013**, *52*, 7261–7265.
- (36) Lee, G. H.; Han, S. H.; Kim, J. B.; Kim, J. H.; Lee, J. M.; Kim, S.-H. Colloidal Photonic Inks for Mechanochromic Films and Patterns with Structural Colors of High Saturation. *Chem. Mater.* **2019**, *31*, 8154–8162.
- (37) Lee, G. H.; Han, S. H.; Kim, D. J.; Lee, S.; Hamonangan, W. M.; Lee, J. M.; Kim, S.-H. Elastic Photonic Microbeads as Building Blocks for Mechanochromic Materials. *ACS Appl. Polym. Mater.* **2020**, 2, 706–714.